PRAMANA
— journal of
physics

© Printed in India

Vol. 46, No. 1,
January 1996
pp. 17–40

On the structure and multipole moments of axially symmetric stationary metrics

S CHAUDHURI and K C DAS
Department of Physics, Gushkara Mahavidyalaya, Gushkara, Burdwan 713 128, India
Department of Physics, Katwa College, Katwa, Burdwan 713 130, India

MS received 5 October 1994

Abstract. The structure of the stationary metrics [1], generated from Laplace's solutions as seed, is investigated. The expressions for the equatorial and polar circumferences, the surface area of the event horizon, location of singular points and the Gaussian curvatures of the metrics [1] are derived and their variations with the field parameter α_0 are studied. The multipole moments are calculated with the help of coordinate invariant Geroch-Hansen technique. These investigations expose some interesting properties of the metrics, some of which are known in the literature and some deserve a new interpretation.

Keywords. General relativity; solutions of Einstein's equations; surface geometry; multipole moments.

PACS No. 04·20

1. Introduction

In a paper [1], we constructed the stationary solutions of Einstein's field equations using two different solutions of Laplace's equation as seed. These solutions describe the real astrophysical objects and reduce to the Kerr metric [2], when some restrictions are imposed on the constants appearing in the solutions. The first one is asymptotically flat and represents the field of a rotating axially symmetric object with mass and higher multipole moments. The second one is not asymptotically flat and may be interpreted as the gravitational field of a rotating object embedded in an external gravitational field. With proper restrictions on the constants, the second solution reduces to the Kerns and Wild metric [3], which is interpreted as Schwarzschild metric embedded in a gravitational field. Both the solutions are not only for a better description of the field of a deformed mass but also for a better description of the gravitational field of a rotating star which is spherically symmetric in its static limit.

In this paper, the structure of our derived metrics [1] is investigated. The location of the event horizon and infinite red shift surface of the metrics are studied. It is found that the event-horizon lies within the infinite red shift surface and both the surfaces, like the Kerr metric, meet at the poles ($\theta = 0, \pi$). The expressions for the surface area and equatorial and polar circumferences are also worked out which give an overall knowledge about the surface deformation. The Gaussian curvatures of our solutions are analyzed. It is found that zones of negative curvature develop around the polar and

equatorial regions when certain restrictions are imposed on the constants α_0 and α. The variations of the surface area, the circumferences and the curvatures with α_0 are thus discussed. The Geroch–Hansen multipole moments [4, 5, 6] of the metric for set-1 are evaluated using Hoenselaers procedure [7]. As set-2 metric is not asymptotically flat, the estimation of its multipole moments is not taken into consideration here.

The mass multipole moments are the measure of deviations from the spherical symmetry of a gravitating body. In all the gravitation theory the mass multipole moment is related to the distribution of matter. Mass multipole moments exist in Newtonian gravitation too. The conventional technique of calculating multipole moments lies in expanding the metric asymptotically. As the general theory of relativity predicts the distortion of curvature of space-time surrounding the object, even an asymptotically flat metric gives rise to a different multipole moment near the body where distortion of curvature is appreciable, compared to the moments calculated from asymptotic expansion. According to Geroch [5], it is very hard to see how this information could be faithfully brought in from infinity over the curved space in order to compare it locally with the matter distribution. As there are equivalent definitions of multipole moments in Newtonian theory e.g. as coefficient in a multipole expansion, as moments of source distribution or objects associated with the conformal group [5], Geroch [5] and Hansen [6] proposed a relativistic and coordinate invariant definition of the multipole moments. The procedure for calculating relativistic moments prescribed by Geroch and Hansen is complicated. Following the prescription of Hoenselaers [8], Quevedo [7] obtained a useful recurrence relation for calculation of higher multipole moments. In this paper, we have followed Quevedo's technique and obtained expressions for coordinate invariant relativistic multipole moments. In § 2, the procedure for calculating Geroch–Hansen (G–H) multipole moments is described in brief. In § 3, the surface geometry of the event-horizon, circumferences and curvatures of our metrics [1] are analyzed and their properties studied. The singularities on the infinite red shift surface are also investigated. Finally the mass multipole moments of the asymptotically flat metric are calculated. In conclusion a discussion of the properties of the metrics is given.

2. Procedure for calculation of G–H multipole moments

For an axially symmetric stationary line element, in prolate spheroidal coordinates (x, y),

$$ds^2 = k^2 f^{-1}\left[e^{2\gamma}(x^2-y^2)\left(\frac{dx^2}{x^2-1}+\frac{dy^2}{1-y^2}\right)+(x^2-1)(1-y^2)d\phi^2\right] - f(dt-wd\phi)^2, \tag{1}$$

the Ernst potential [9, 10] is defined as

$$E = f + i\Phi, \tag{2}$$

where, k is a constant, f, γ, w and Φ are functions of (x, y) only. Φ is known as the twist potential. The prolate spheroidal coordinates (x, y) are related to Papapetrou coordinates (ρ, z) by

$$\rho^2 = k^2(x^2-1)(1-y^2), \tag{3}$$

$$z = kxy. \tag{4}$$

Another Ernst potential ξ is defined as [9, 10]

$$\xi = \frac{1-E}{1+E}, \tag{5}$$

Weyl canonical coordinate by

$$\bar{z} = \frac{1}{z} = \frac{1}{kxy} \tag{6}$$

and the conformally transformed potential $\bar{\xi}$ on the symmetry axis $y = 1$, is defined by

$$\bar{\xi}(\bar{z}, 1) = \frac{1}{\bar{z}} \xi(\bar{z}, 1). \tag{7}$$

With the above substitution, Hoenselaers listed the expressions for mass multipole moments (M_l) and current multipole moments (J_l) of the source as

$$M_l = \mathrm{Re}(m_l + \mathrm{d}_l), \tag{8}$$

$$J_l = \mathrm{Im}(m_l + \mathrm{d}_l), \tag{9}$$

where,

$$m_l = \frac{1}{l!} \frac{\mathrm{d}^l \bar{\xi}(\bar{z}, 1)}{\mathrm{d}\bar{z}^l}\bigg|_{\bar{z}=0}. \tag{10}$$

$d_l (l = 0, 1, 2, 3, \ldots)$ is determined by comparing (8) and (9) with the original Geroch–Hansen definition. According to them d_l can be expressed in terms of m_k for $k \leqslant l-1$. The first six values of d_l are

$$\mathrm{d}_0 = \mathrm{d}_1 = \mathrm{d}_2 = \mathrm{d}_3 = 0, \quad \mathrm{d}_4 = \frac{1}{7} m_0^* (m_1^2 - m_2 m_0),$$

$$\mathrm{d}_5 = \frac{1}{3} m_0^* (m_2 m_1 - m_3 m_0) + \frac{1}{21} m_1^* (m_1^2 - m_2 m_0). \tag{11}$$

Expanding ξ in powers of $\bar{z}$, one obtains

$$\xi(\bar{z}, 1) = \sum_{k=1}^{\infty} \frac{\mathrm{d}^k \xi(\bar{z}, 1)}{\mathrm{d}\bar{z}^k}\bigg|_{\bar{z}=0} \frac{\bar{z}^k}{k!}, \tag{12}$$

and from (10) and (7):

$$m_l = \frac{1}{(l+1)!} \frac{\mathrm{d}^{l+1} \xi(\bar{z}, 1)}{\mathrm{d}\bar{z}^{l+1}}\bigg|_{\bar{z}=0} \tag{13}$$

Substituting the value of ξ from (5) in (13), an important recurrence formula for m_l is obtained

$$m_l = -\frac{h_{l+1}}{(l+1)!}\bigg|_{\substack{y=1 \\ \bar{z}=0}}, \tag{14}$$

where

$$h_1 = \frac{1}{2E} \frac{\mathrm{d}E}{\mathrm{d}\bar{z}} \tag{15}$$

and

$$h_l = \frac{\mathrm{d}h_{l-1}}{\mathrm{d}\bar{z}} + 2\xi h_1 h_{l-1}, \quad \text{for} \quad 1 \geqslant 2. \tag{16}$$

For static metric, $f = e^{2\psi}$, $\Phi = 0$ and $k = m$, the above calculation becomes a simple task.

In general, Quevedo [7] summarized the above procedure as follows. (1) Calculate Ernst potential E and ξ according to (2) and (5), (2) Calculate m_l according to (14), (3) Obtain multipole moments from (8), (9) and (11).

3. On the surface geometry of event-horizon and multipole moments

In this section, the structure of our metrics [1] is investigated. The equatorial and polar circumferences, the surface area of the event-horizon and the Gaussian curvatures at the polar and equatorial regions are computed. It is shown that the superposing field plays an important role on the shape of the infinite red shift surface. Negative curvature zones are found to exist under certain restrictions on the values of the constants α_0 and α. The mass multipole moments and the current multipole moments are derived for an asymptotically flat stationary solution. The multipole moments differ much from the moments of Kerr.

The axially symmetric line element is written in the form as in eq (1). The metric functions f, γ and w are given in ref. [1].

According to Gutsunaev and Manko [11], the Ernst potential $E = f + i\phi$, can be expressed as

$$E = e^{2\psi}\frac{x(1+ab) + iy(b-a) - (1-ia)(1-ib)}{x(1+ab) + iy(b-a) + (1-ia)(1-ib)}, \tag{17}$$

where a and b are derived from two pairs of first order differential equations given in [11, 1]; 2ψ is the Laplace's solution. Thus different solutions of Laplace's equation will render different solutions of the axially symmetric field equations.

We considered the following cases in ref. [1].

Set 1: Laplace's solution

$$2\psi = \alpha_0(x+y)^{-1}, \tag{18}$$

where α_0 is a constant,

$$a = -\alpha\exp[\alpha_0 y(x+y)^{-1}], \tag{19}$$

$$b = \alpha\exp[-\alpha_0(1+xy)(x+y)^{-2}], \tag{20}$$

$$f = e^{\alpha_0/(x+y)}A/B, \tag{21}$$

$$e^{2\gamma} = k_1 A(x^2-y^2)^{-1}\exp\left[\frac{\alpha_0}{4}(x+y)^{-4}(1-y^2)\{4(x+y)^2 - \alpha_0(x^2-1)\}\right], \tag{22}$$

$$w = 2k e^{-\alpha_0/(x+y)}CA^{-1} + k_2, \tag{23}$$

where k_1, k_2 are new constants. A, B, C are given by

$$A = (x^2-1)[1-\alpha^2 e^{-\alpha_0((1-y^2)/(x+y)^2)}]^2 - \alpha^2(1-y^2) \times [e^{\alpha_0 y/(x+y)} + e^{(-\alpha_0(xy+1))/(x+y)^2}]^2, \tag{24}$$

$$B = [(x+1)-\alpha^2(x-1)e^{(-\alpha_0(1-y^2))/(x+y)^2}]^2 + \alpha^2[(1-y)e^{(-\alpha_0(xy+1))/(x+y)^2} - (1+y)e^{\alpha_0 y/(x+y)}]^2, \tag{25}$$

$$C = \alpha(x^2-1)[1-\alpha^2 e^{(-\alpha_0(1-y^2))/(x+y)^2}][e^{(-\alpha_0(xy+1))/(x+y)^2} + e^{\alpha_0 y/(x+y)} - y(e^{(-\alpha_0(xy+1))/(x+y)^2} - e^{\alpha_0 y/(x+y)})] + \alpha(1-y^2)[e^{(-\alpha_0(xy+1))/(x+y)^2} + e^{\alpha_0 y/(x+y)}] \times [(1-\alpha^2 e^{(-\alpha_0(1-y^2))/(x+y)^2}) + x(1+\alpha^2 e^{(-\alpha_0(1-y^2))/(x+y)^2})]. \tag{26}$$

(a) *Singularities, infinite red shift surface and event-horizon*

A preliminary analysis of our metric (21)–(26) was published in [1]. Computer analysis shows that the metric retains its singularity at the poles $x = \pm 1$, $y = \pm 1$, and for a constant value of y, the location of x-coordinate of singular points changes with the variations of α_0 and α. On the equatorial plane ($y = 0$), and planes adjacent to the equator ($0{\cdot}5 \geqslant y > 0$), for a constant value of α, the singular points come closer to $x = 1$ value when α_0 is increased. When $y > 0{\cdot}5$ the x-coordinate of singularity first decreases and then increases with the increase in α_0. It is also observed that for a constant value of α, the range of x-coordinate of singular points decreases when y is increased from 0 to 1. It is interesting that for $y \sim 0{\cdot}9$ and $\alpha \leqslant 0{\cdot}5$, singular point shifts away from the origin when α_0 is gradually increased, while for $y = 0{\cdot}9$ and $\alpha = 0{\cdot}9$, the x-coordinate of singularity decreases with increase in α_0. The location of singular points are shown in figures 1(a)–(e), for pre-assigned values of α_0 and α.

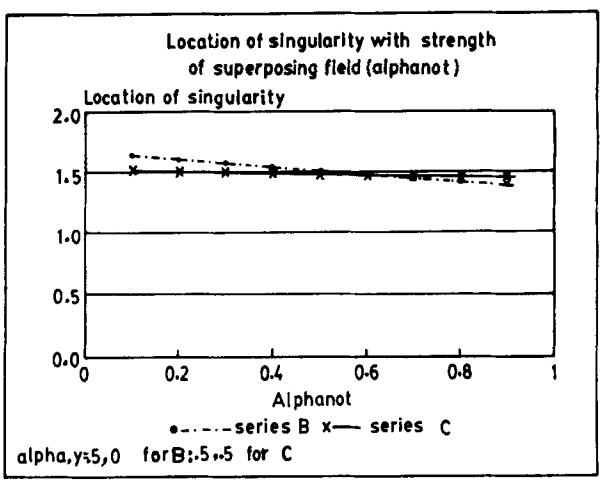

Figure 1(a). Graphs illustrating the locus of singular points due to the variations of the strength of the superposing field (α_0). Figure shows that the singular points come closer to $x = 1$, for different set of values of α and y (here $\alpha = 0{\cdot}5$, $y = 0$ for series B and $\alpha = 0{\cdot}5$, $y = 0{\cdot}5$ for series C) when α_0 is increased from 0·1 to 0·9.

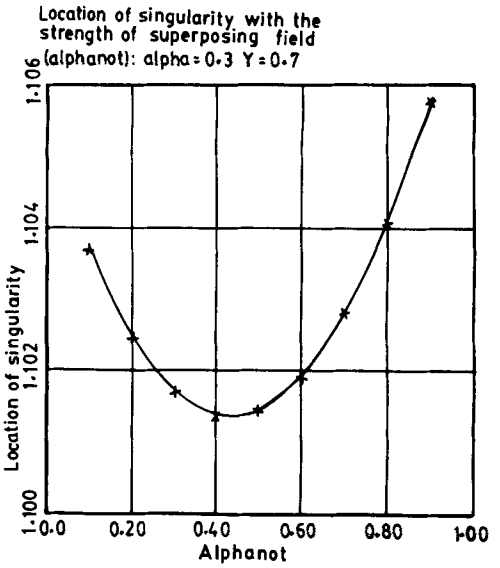

Figure 1(b). A plot showing the locus of singularities against the variation of α_0, with constant α and y (we have taken $\alpha = 0{\cdot}3$, $y = 0{\cdot}7$). Singular points are found to come closer to $x = 1$ value and then goes away from it.

When the values of α_0 and α ($\alpha \leqslant 0{\cdot}5$) are kept fixed, it is found that with the increment in the value of y, the location of singular point increases slightly beyond $x = 1$ value and then comes closer to $x = 1$, However, for $\alpha > 0{\cdot}5$, the x-coordinate of singular point is a decreasing function of y. These are illustrated in figures 2(a) and 2(b). With constant α_0 and y, as the value of α increases, the singular point shifts away from $x = 1$ value.

Our metric shows two important surfaces, namely, the event-horizon and the infinite red shift surface enclosing the event-horizon. The existence of the event-horizon is an important factor for a black hole which according to Penrose is the boundary of the asymptotic region from which time-like curves may escape to infinity [12]. An event-horizon is always a null hypersurface and more than one may be present there. It is a one way path and there may occur a naked singularity in the absence of an event-horizon. The event-horizon of the metric (1) is at $x = x_{\text{hor}} = 1$.

The infinite red shift surface can be obtained by equating

$$f = 0 \tag{27}$$

in (21). Static sources and observers can stay only outside the above surface and not on or inside it. From (21), (24), (25) and (27), it is found that $x_{\text{i.r.s.}} = x(y)$ and $x_{\text{i.r.s.}} > x_{\text{hor}}$ for $|y| < 1$. However at the poles $y = \pm 1$, the infinite red shift surface and the event-horizon touches each other. Thus the event-horizon is always covered by the infinite red shift surface similar to the Kerr metric and the ergosphere (i.e. the region in between the infinite red shift surface and event-horizon) has analogous properties to that of Kerr metric.

(b) *Surface area, polar and equatorial circumferences*

At event-horizon i.e. at $x = 1$ and $t =$ constant, our metric (1) can be treated as a two

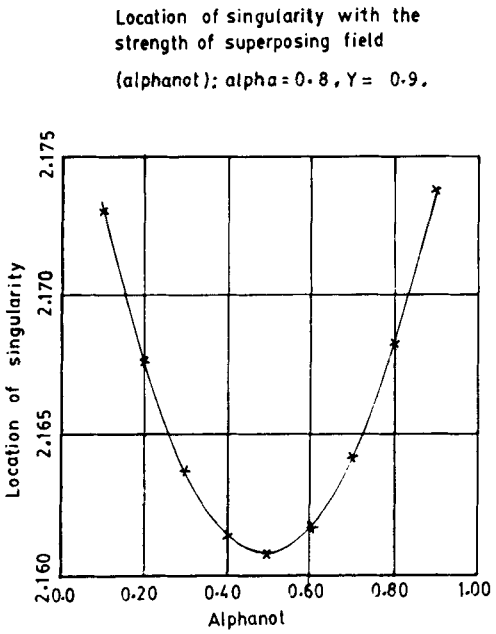

Figure 1(c). Figure shows the shift in the location of singular points with the variation of α_0 ($\alpha = 0{\cdot}8$, $y = 0{\cdot}9$ are kept constants).

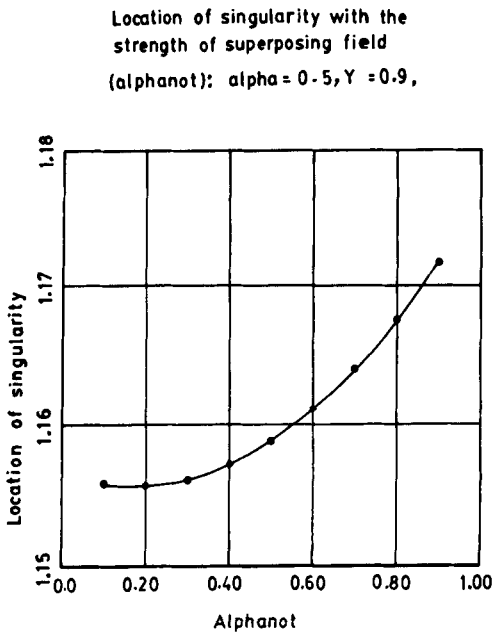

Figure 1(d). The variation of the location of singular points with α_0 (for $\alpha = 0{\cdot}5$, $y = 0{\cdot}9$) are plotted. Singular points are found to shift away from $x = 1$ value.

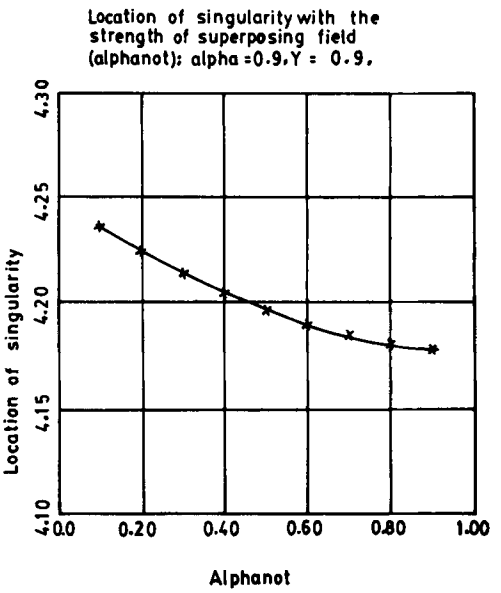

Figure 1(e). Graph illustrating the locus of singular points due to the variation of α_0 (for $\alpha = 0{\cdot}9$, $y = 0{\cdot}9$). As α_0 increases, singular points come closer to $x = 1$.

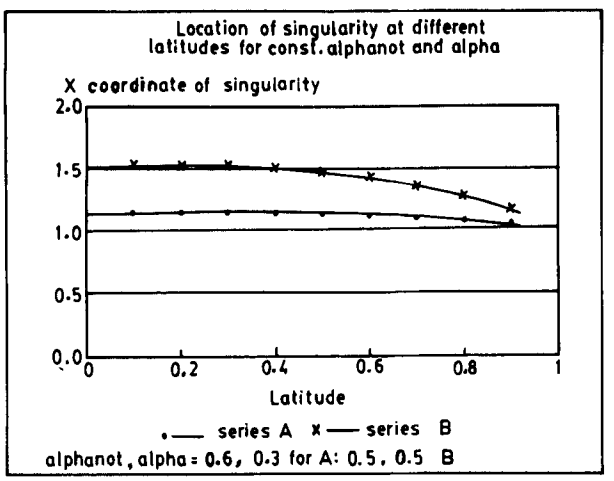

Figure 2(a). Graphical illustration showing the influence of external field on the shape of the infinite red shift surface. For $\alpha_0 = 0{\cdot}6$, $\alpha = 0{\cdot}3$, $\alpha_0 = 0{\cdot}5$ and $\alpha = 0{\cdot}5$, the infinite red shift surfaces are shown in series A and B respectively.

dimensional line element which under the coordinate transformation

$$y = \cos\theta, \tag{28}$$

$$k_1 = (1-\alpha^2)^{-2} \quad \text{and} \quad k_2 = -4k\alpha(1-\alpha^2)^{-1}, \tag{29}$$

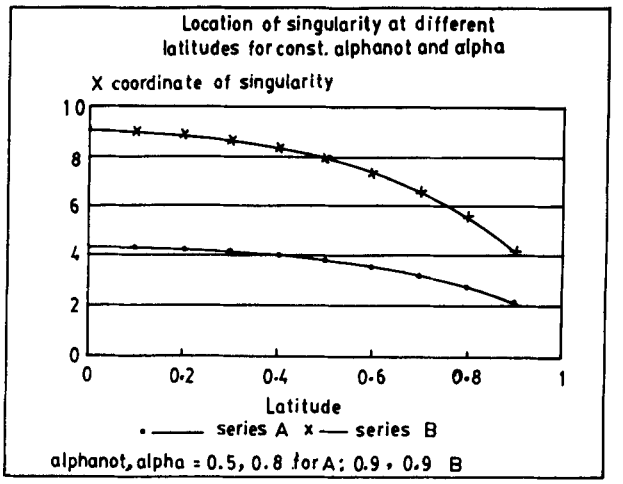

Figure 2(b). Another plot showing the shape of infinite red shift surface for constant values of α_0 and α ($\alpha_0 = 0{\cdot}5$, $\alpha = 0{\cdot}8$ for series A and $\alpha_0 = 0{\cdot}9$, $\alpha = 0{\cdot}9$ for series B).

assumes the form

$$ds^2 = g_{\theta\theta}d\theta^2 + g_{\phi\phi}d\phi^2, \tag{30}$$

where

$$g_{\theta\theta} = \frac{k^2}{(1-\alpha^2)^2} H e^{-\alpha_0/(1+\cos\theta)}, \tag{31}$$

$$g_{\phi\phi} = 16k^2 \frac{(1+\alpha^2 e^{\alpha_0})^2}{(1-\alpha^2)^2} \frac{\sin^2\theta}{H} e^{-\alpha_0\cos\theta/(1+\cos\theta)}, \tag{32}$$

and

$$H = \alpha^2[(1+\cos\theta)e^{\alpha_0/2} - (1-\cos\theta)e^{-\alpha_0/2}]^2 + 4e^{(\alpha_0(1-\cos\theta))/(1+\cos\theta)}. \tag{33}$$

The surface area of the event-horizon can be evaluated from the integral [13]

$$S = \int_0^{\pi}\int_0^{2\pi} \sqrt{g_{\theta\theta}g_{\phi\phi}}\, d\theta d\phi. \tag{34}$$

Integrating for metric (31)–(33), we obtain

$$S = 16\pi k^2 \frac{(1+\alpha^2 e^{\alpha_0})}{(1-\alpha^2)^2} e^{-\alpha_0/2}. \tag{35}$$

The surface area thus increases with α_0. On substituting $\alpha_0 = 0$, (35) reduces to the familiar Kerr expression, $S = 8\pi m(m + (m^2 - a^2)^{1/2})$. For $\alpha_0 = \alpha = 0$, Schwarzschild expression, $S = 16\pi m^2$ is reproduced.

The latitudinal circumference (i.e. the curcumference at different latitude) can be obtained from the integral

$$A_1 = \int_0^{2\pi} \sqrt{g_{\phi\phi}}\, d\phi, \tag{36}$$

and is found to be

$$A_1 = 8\pi k \frac{(1+\alpha^2 e^{\alpha_0})}{(1-\alpha^2)} \times \frac{\sin\theta e^{(-\alpha_0\cos\theta)/2(1+\cos\theta)}}{[\alpha^2\{(1+\cos\theta)e^{\alpha_0/2} - (1-\cos\theta)e^{-\alpha_0/2}\}^2 + 4e^{(\alpha_0(1-\cos\theta))/(1+\cos\theta)}]^{1/2}}. \quad (37)$$

Here, $\theta = \pi/2$ represents the equator and $\theta = 0$, π are the upper and lower poles respectively. One thus obtains the expression for equatorial circumference as

$$A_e(\theta = \tfrac{\pi}{2}) = 8\pi k \frac{(1+\alpha^2 e^{\alpha_0})}{(1-\alpha^2)[\alpha^2\{e^{\alpha_0/2} - e^{-\alpha_0/2}\}^2 + 4e^{\alpha_0}]^{1/2}}. \quad (38)$$

Equation (38) reduces to the corresponding Kerr expression for $\alpha_0 = 0$ and to the Schwarzschild for $\alpha_0 = 0$, $\alpha = 0$.

The polar circumference (A_p) can be computed from the relation

$$A_p = \int_0^{2\pi} \sqrt{g_{\theta\theta}}\, d\theta. \quad (39)$$

For metric (30) given by (31)–(33), it is found that

$$A_p = \frac{k}{(1-\alpha^2)} \int_0^{2\pi} [\alpha^2\{(1+\cos\theta)e^{(\alpha_0\cos\theta)/2(1+\cos\theta)} - (1-\cos\theta)e^{(-\alpha_0(2+\cos\theta))/2(1+\cos\theta)}\}^2 + 4e^{-\alpha_0\cos\theta/(1+\cos\theta)}]^{1/2} d\theta. \quad (40)$$

Evaluation of the integral (40) is not simple. In order to get the exact variations of A_1, A_e and A_p with α_0, (37), (38) and (40) are analyzed using computer. It is found that for

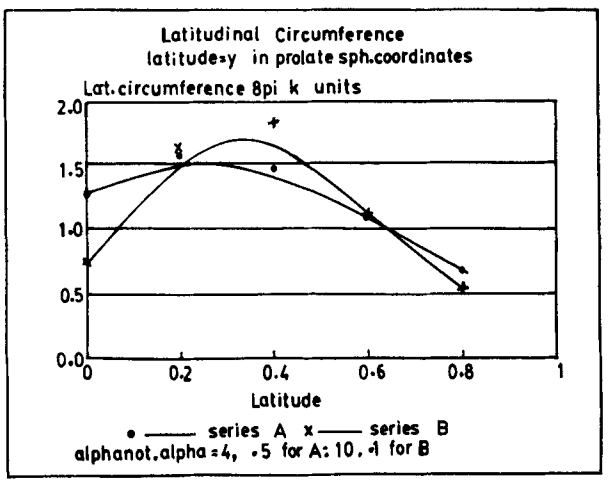

Figure 3(a). The plot shows the changes of circumference at different latitudes for constant values of α_0 and α ($\alpha_0 = 4, \alpha = 0{\cdot}5$ for series A and $\alpha_0 = 10, \alpha = 0{\cdot}1$ for series B). The infinite red shift surface assumes a dumb-bell structure.

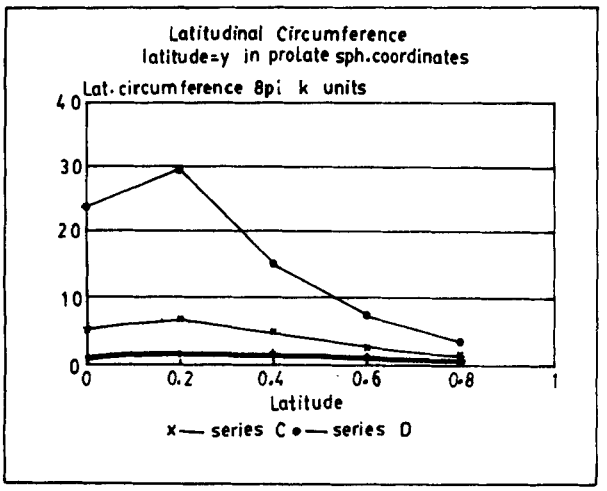

Figure 3(b). Curves represent the variation of latitudinal circumferences for constant values of α_0 and α. The assumed values of α_0 and α are 7, 0·5 and 10, 0·5 for series C, and D respectively.

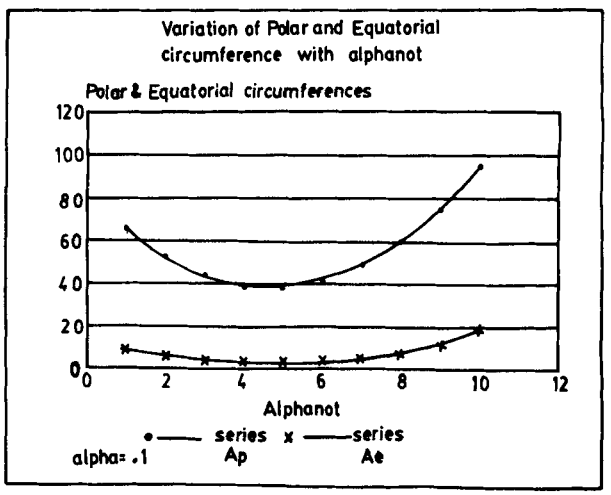

Figure 4(a). With constant α ($\alpha = 0{\cdot}1$), the nature of variations of polar and equatorial circumferences with the strength of the superposing field (α_0) are shown. The upper curve represents polar circumference (A_p) and the lower one is for equatorial circumference (A_e). A_p always remains larger than A_e.

constant values of α_0 and α, the latitudinal circumference first increases with the latitude and then decreases. The locus of the points on the infinite red shift surface or perhaps the body itself assumes a dumbbell structure. The deformation is different for different sets of values of α_0 and α as illustrated in figures 3(a) and 3(b). It is also noted that for a constant value of α (but for $\alpha \leqslant 0{\cdot}5$), when α_0 is gradually increased, the equatorial and polar circumferences first decrease and then increase with α_0 and

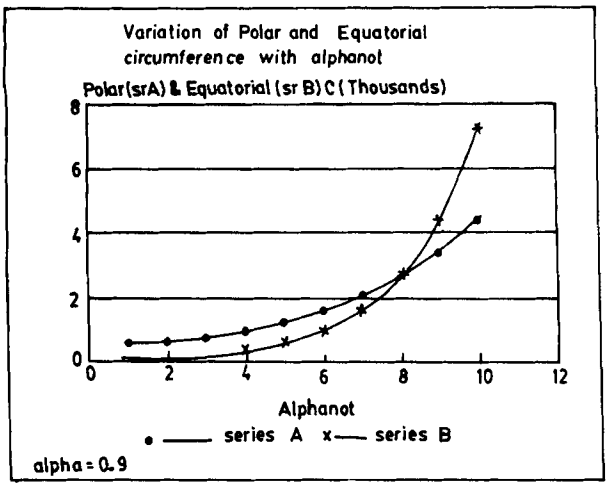

Figure 4(b). A set of curves, showing the polar (A_p) and equatorial (A_e) circumferences, are given. For $\alpha = 0{\cdot}9$ and $\alpha_0 > 8$, A_e exceeds A_p.

A_p always remains larger than A_e. However, when $\alpha > 0{\cdot}5$, both A_p and A_e are increasing functions of α_0. But the rate of increase of A_e is larger than that of A_p. When $\alpha_0 \gtrsim 8$, the equatorial circumference becomes larger than the polar circumference. The exact value of α_0 for which A_e exceeds A_p depends on the value of α. Figures 4(a) and 4(b) show variations of polar and equatorial circumferences with α_0. With α_0 constant both A_p and A_e increases with the increase in α.

The nature of variation of x with α_0, α or y as observed in the above analysis points to the deformation of the infinite red shift surface and perhaps of the body itself to which the field is due.

Astrophysical objects are not isolated in space. They are embedded in external gravitational as well as electromagnetic field and thus our above analysis bears some relevance to those objects. However, the exact correspondence is yet to be discovered.

(c) *Gaussian curvature*

The Gaussian curvature is a measure of geometry intrinsic to the horizon and it is independent of embedding space. The Gaussian curvature of the metric (30) can be computed from the relation [14]

$$C = -\frac{1}{2EG}\frac{\mathrm{d}}{\mathrm{d}\theta}\left(\frac{1}{EG}\frac{\mathrm{d}G^2}{\mathrm{d}\theta}\right), \tag{41}$$

where

$$E = \sqrt{g_{\theta\theta}}, \quad G = \sqrt{g_{\phi\phi}}. \tag{42}$$

The Gaussian curvature in this case becomes

$$C = \frac{(1-\alpha^2)^2 e^{\alpha_0}}{2k^2}\frac{1}{B_1^3}[B_1B_3B_4 + B_1B_2B_6 - 2B_2B_3B_5] \tag{43}$$

where

$$B_1 = \alpha^2(b_1 + 2b_2\cos\theta + b_3\cos^2\theta) + 4e^{\alpha_0(1-\cos\theta)/(1+\cos\theta)},$$

$$B_2 = e^{-(\alpha_0\cos\theta)/(1+\cos\theta)},$$

$$B_3 = 2\alpha^2[b_2 + (b_1 + b_3)\cos\theta + b_2\cos^2\theta] + \alpha_0\left(\frac{1-\cos\theta}{1+\cos\theta}\right)B_1$$
$$+ 8e^{\alpha_0(1-\cos\theta)/(1+\cos\theta)}\left[\cos\theta - \alpha_0\frac{(1-\cos\theta)}{(1+\cos\theta)}\right],$$

$$B_4 = -\frac{\alpha_0}{(1+\cos\theta)^2}e^{-\alpha_0\cos\theta/(1+\cos\theta)},$$

$$B_5 = 2\alpha^2(b_2 + b_3\cos\theta) - \frac{8\alpha_0}{(1+\cos\theta)^2}e^{\alpha_0(1-\cos\theta)/(1+\cos\theta)},$$

$$B_6 = 2\alpha^2(b_1 + b_3 + 2b_2\cos\theta) - \frac{2\alpha_0}{(1+\cos\theta)}B_1 + \frac{\alpha_0(1-\cos\theta)}{(1+\cos\theta)}B_5$$
$$- \frac{16\alpha_0}{(1+\cos\theta)^2}\left[\cos\theta - \alpha_0\frac{(1-\cos\theta)}{(1+\cos\theta)}\right]e^{\alpha_0(1-\cos\theta)/(1+\cos\theta)}$$
$$+ 8\left[1 + \frac{2\alpha_0}{(1+\cos\theta)^2}\right]e^{\alpha_0(1-\cos\theta)/(1+\cos\theta)}, \tag{44}$$

and

$$b_1 = (e^{\alpha_0/2} - e^{-\alpha_0/2})^2,$$

$$b_2 = (e^{\alpha_0} - e^{-\alpha_0}),$$

$$b_3 = (e^{\alpha_0/2} + e^{-\alpha_0/2})^2. \tag{45}$$

On substituting $\alpha_0 = 0$ and $\alpha_0 = \alpha = 0$, (43) reduces to the corresponding expressions for Kerr and Schwarzschild metrics respectively. The curvature is found to be a function of polar angle.

At the pole $\theta = 0$, the curvature becomes

$$C_{\theta=0} = \frac{(1-\alpha^2)^2 e^{\alpha_0/2}}{8k^2(1+\alpha^2 e^{\alpha_0})^2}[(\alpha_0 + 2)(1 - \alpha^2 e^{\alpha_0}) - 4\alpha^2]. \tag{46}$$

In the polar region, where α_0 and α satisfy the relation

$$(\alpha_0 + 2)(1 - \alpha^2 e^{\alpha_0}) = 4\alpha^2, \tag{47}$$

the curvature is zero and the surface in that region becomes a plane.

A zone of negative curvature develops around the pole $\theta = 0$, if the values of α_0 and α are such that

$$(\alpha_0 + 2)(1 - \alpha^2 e^{\alpha_0}) < 4\alpha^2, \tag{48}$$

provided $\alpha^2 e^{\alpha_0} < 1$. If $\alpha^2 e^{\alpha_0} > 1$, the curvature will always be negative. The negative curvature cannot be visualized because it cannot be embedded in a flat Euclidean space.

Thus depending on the values of α_0 and α, we have two geometrically distinct classes of the gravitational mass. The first type consists of a deformed sphere with which we are accustomed to in the usual three dimensional Euclidean space. They have positive curvature everywhere. The second type is very unusual in our familiar three dimensional space. They possess negative Gaussian curvature and global embedding is not possible for surfaces having $C < 0$.

Since there exists a singularity at the pole $\theta = \pi$ (i.e. at $x = 1$, $y = -1$), it is very difficult to investigate the nature of curvature at that pole with a computer.

At the equator $\theta = \pi/2$, the curvature can be written in the form

$$C_{\theta=\pi/2} = \frac{(1+\alpha^2)^2 e^{\alpha_0}}{2k^2 p^3}[(2 - 2\alpha_0 - \alpha_0^2)P^2 + (R - 8\alpha_0 Q)P - 8Q^2], \tag{49}$$

where

$$P = b_1\alpha^2 + 4e^{\alpha_0},$$

$$Q = b_2\alpha^2 - 4\alpha_0 e^{\alpha_0},$$

$$R = 2b_3\alpha^2 + 16\alpha_0(1+\alpha_0)e^{\alpha_0}. \tag{50}$$

It is very difficult to predict the nature of variation of equatorial curvature with α_0. However, a computer analysis shows that for a constant value of α, $C_{\theta=\pi/2}$ is an increasing function of α_0. Figure 5 shows the plot of equatorial curvature with the variations of α_0. Further it is found that for fixed α_0, equatorial curvature increases with the increase in α.

(d) *Multipole moments*

It has been shown in our earlier paper [1] that (19) to (26) determine our new stationary metric (1) completely. With $\alpha_0 = \alpha = 0$, our metric reduces to the Schwarzschild

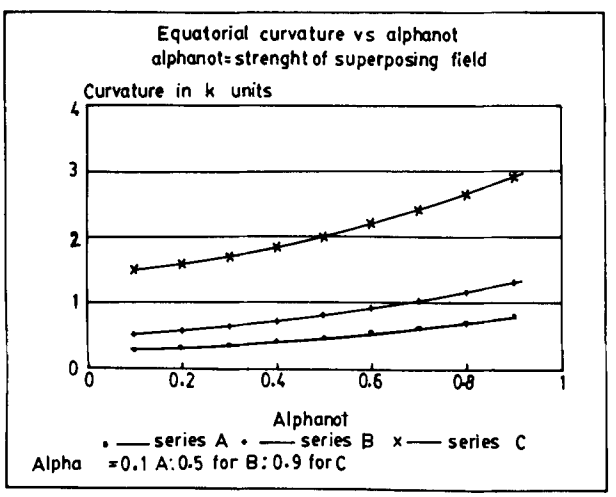

Figure 5. A plot of equatorial curvature (C_e) with the strength of the external field is shown. C_e is an increasing function of α_0. The values of α taken are 0·1 for series A, 0·5 for series B and 0·9 for series C.

solution. Further, with $\alpha_0 = 0$, $\alpha \neq 0$, and with the substitution

$$kx = r - m, \quad y = \cos\theta, \quad k = mp, \quad a = mq,$$
$$k^2 = m^2 - a^2, \quad p = (1-\alpha^2)(1+\alpha^2)^{-1}, \quad q = 2\alpha(1+\alpha^2)^{-1}.$$

Kerr metric is obtained in its standard form. When no restrictions are imposed on the constants i.e. $\alpha_0 \neq 0$, $\alpha \neq 0$, the solution given by (19)–(26), generalizes the Kerr metric with an arbitrary set of multipole moments determined by the parameter α_0. The first four coordinate invariant relativistic Geroch–Hansen [5, 6] multipole moments characterizing the mass and angular momentum distributions are computed as follows

$$M_0 = k\left[\frac{(1+\alpha^2)}{(1-\alpha^2)} - \frac{\alpha_0}{2}\right],$$
$$M_1 = k^2\left(\frac{\alpha_0}{2}\right),$$
$$M_2 = k^3\left[-\frac{\alpha_0^3}{3} + \left\{3\left(\frac{\alpha_0}{2}\right) - \left(\frac{1+\alpha^2}{1-\alpha^2}\right)\right\}\left\{\left(\frac{\alpha_0}{2}\right)^2 + 4\alpha^2(1-\alpha^2)^{-2}\right\}\right],$$
$$M_3 = k^4\left(\frac{\alpha_0}{2}\right)\left[-\left(\frac{\alpha_0}{2}\right)^2 + \{4\alpha^2(1-\alpha_0) - 3\alpha^4(1+2\alpha_0) + 3\}(1-\alpha^2)^{-2}\right], \tag{51}$$

$$J_0 = 0,$$
$$J_1 = 2k^2\alpha[\alpha_0(1-\alpha^2) - (1+\alpha^2)](1-\alpha^2)^{-2},$$
$$J_2 = -2k^3\alpha\alpha_0(1-\alpha^2)^{-1},$$
$$J_3 = k^4\alpha\left[\frac{\alpha_0^2}{6}\{9(1-\alpha^4) - \alpha_0(1-\alpha^2)^2\}\right.$$
$$\left. + 2\alpha^2\{\alpha_0(1-\alpha^2)(9-\alpha^4) - 4(1+\alpha^2)\}\right](1-\alpha^2)^{-4}. \tag{52}$$

Since $J_0 = 0$, the metric obtained is asymptotically flat [15]. With $\alpha_0 = 0$, the multipole moments so obtained reduce to that of Kerr and the mass monopole term becomes equal to the total mass of the source.

A computer calculation for the variation of mass multipole moments with the strength of the superposing field (α_0) shows that the monopole moment (M_0) decreases with increase in α_0 while the dipole moment (M_1) increases. For a constant value of α (we have taken $\alpha = 0{\cdot}9$), these two moments M_0 and M_1 becomes equal when $\alpha_0 \approx 9{\cdot}5$. As regards to quadrupole (M_2) and octupole (M_3) moments it is found that the former increases with α_0 while the latter is a decreasing function of α_0. The variations of mass multipole moments with the external field parameter α_0 are shown in figures 6(a) and 6(b).

On the other hand, with constant α_0, the monopole moment increases with the increase in the rotation parameter α, while the dipole moment is independent of it. The quadrupole moment first increases with the increase in α and then decreases for values of α_0 lying in the range $1 \leqslant \alpha_0 < 8$. When $\alpha_0 \geqslant 8$, M_2 increases with α. The octupole moment is a decreasing function of α.

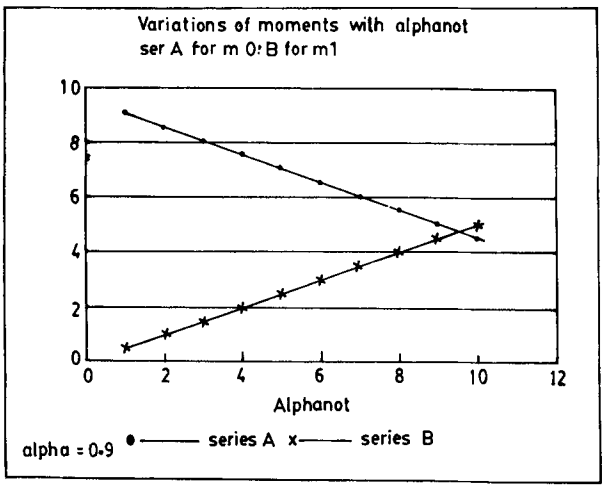

Figure 6(a). The graph shows the variations of monopole (M_0) and dipole (M_1) moments with α_0, keeping α constant (here we have taken $\alpha = 0{\cdot}9$). Series A represents monopole moment and series B for dipole moment.

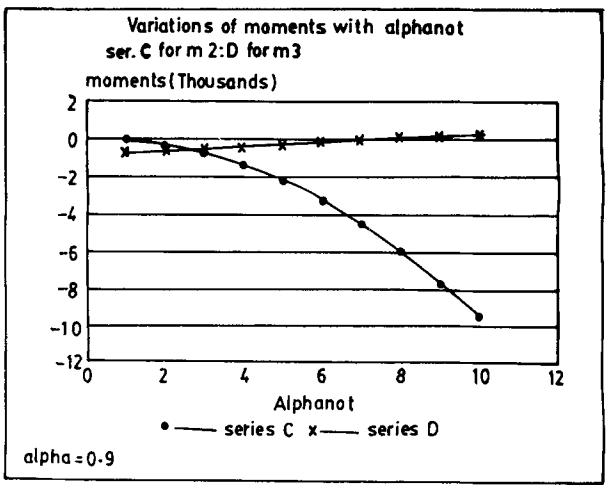

Figure 6(b). Variations of quadrupole (series C) and octupole (series D) moments with α_0 are plotted (for $\alpha = 0{\cdot}9$).

Set 2: Let us take another Laplace's solution

$$2\psi = \alpha_0 xy. \tag{53}$$

a and b were found to be [1]

$$a = -\alpha \exp[\alpha_0 z_0 (x - y)], \tag{54}$$

$$b = \alpha \exp[-\alpha_0 z_0 (x + y)], \tag{55}$$

where z_0 is another constant. The metric functions f, w and γ, as in set 1, are given by [1]

$$f = A/B\exp(\alpha_0 xy), \tag{56}$$

$$w = 2kCA^{-1}\exp(-\alpha_0 xy) + k_2, \tag{57}$$

$$e^{2\gamma} = k_1 A(x^2 - y^2)^{-1}\exp[2\alpha_0 y - \frac{\alpha_0^2}{4}(x^2 - 1)(1 - y^2)], \tag{58}$$

where k_1 and k_2 are constants and A, B, C are given by

$$A = e^{-2\alpha_0 z_0 y}[(x^2 - 1)(e^{\alpha_0 z_0 y} - \alpha^2 e^{-\alpha_0 z_0 y})^2 - \alpha^2(1 - y^2)(e^{\alpha_0 z_0 x} + e^{-\alpha_0 z_0 x})^2], \tag{59}$$

$$B = e^{-2\alpha_0 z_0 y}\{[(x + 1)e^{\alpha_0 z_0 y} - \alpha^2(x - 1)e^{-\alpha_0 z_0 y}]^2 + \alpha^2[(1 + y)e^{\alpha_0 z_0 x} - (1 - y)e^{-\alpha_0 z_0 x}]^2\}, \tag{60}$$

$$C = \alpha e^{-2\alpha_0 z_0 y}[(x^2 - 1)(e^{\alpha_0 z_0 y} - \alpha^2 e^{-\alpha_0 z_0 y}) \times \{e^{\alpha_0 z_0 x} + e^{-\alpha_0 z_0 x} - y(e^{-\alpha_0 z_0 x} - e^{\alpha_0 z_0 x})\} + (1 - y^2)(e^{\alpha_0 z_0 x} + e^{-\alpha_0 z_0 x}) \times \{e^{\alpha_0 z_0 y} - \alpha^2 e^{-\alpha_0 z_0 y} + x(e^{\alpha_0 z_0 y} + \alpha^2 e^{-\alpha_0 z_0 y})\}]. \tag{61}$$

(a) *Infinite red shift surface, event-horizon and singularities*

The event-horizon of our metric (1) is at $x = x_{\text{hor}} = 1$ and the infinite red shift surface is obtained by equating $f = 0$ in (56). At the poles $y = \pm 1$, $x = 1$, i.e. the event-horizon and the infinite red shift surface coincide. However, for values of $|y| < 1$, $x_{\text{i.r.s.}} > x_{\text{hor}}$, and the ergosphere possesses Kerr-like properties.

The reported metric is singular at the poles $x = \pm 1$, $y = \pm 1$, and at least one singular point exists on the equatorial plane $y = 0$. With proper restrictions on the constants α_0 and α, our derived metric reduces to the different well-known metrics such as Schwarzschild, Kerr and Kerns and Wild.

(b) *Surface area, polar and equatorial circumferences*

At event-horizon i.e. at $x = 1$, our metric (1) with $2\psi = \alpha_0 xy$, assumes the form of a two dimensional line element,which on substitution

$$y = \cos\theta \tag{62}$$

and

$$k_1 = (1 - \alpha^2)^{-2}, \quad k_2 = -4k\alpha(1 - \alpha^2)^{-1}, \quad z_0 = 1,$$

can be written as

$$ds^2 = g_{\theta\theta}d\theta^2 + g_{\phi\phi}d\phi^2, \tag{63}$$

where

$$g_{\theta\theta} = \frac{k^2}{(1 - \alpha^2)^2}H' e^{-\alpha_0 \cos\theta}, \tag{64}$$

$$g_{\phi\phi} = 16k^2 \frac{(1-\alpha^2+\beta\alpha^2)^2}{(1-\alpha^2)^2} \frac{\sin^2\theta e^{\alpha_0\cos\theta}}{H'}, \tag{65}$$

$$H' = \alpha^2[(1+\cos\theta)e^{\alpha_0} - (1-\cos\theta)e^{-\alpha_0}]^2 + 4e^{2\alpha_0\cos\theta}, \tag{66}$$

$$\beta = e^{\alpha_0} + e^{-\alpha_0}. \tag{67}$$

The surface area of the event-horizon is obtained as

$$S = 16\pi k^2 \frac{(1-\alpha^2+\beta\alpha^2)}{(1-\alpha^2)^2}. \tag{68}$$

The surface area thus increases with increase in the strength of the superposing field (α_0). On substituting $\alpha_0 = 0$, (67) reduces to that of Kerr and with $\alpha_0 = \alpha = 0$, Schwarzschild's expression $S = 16\pi m^2$ is obtained.

The latitudinal circumference (A_1) is computed from (36) and is found to be

$$A_1 = 8\pi k \frac{(1-\alpha^2+\beta\alpha^2)}{(1-\alpha^2)} \frac{\sin\theta e^{(1/2)(\alpha_0\cos\theta)}}{[\alpha^2\{(1+\cos\theta)e^{\alpha_0} - (1-\cos\theta)e^{-\alpha_0}\}^2 + 4e^{2\alpha_0\cos\theta}]^{1/2}}. \tag{69}$$

With $\theta = \pi/2$, one obtains the expression for circumference at the equator. A computer analysis shows that with α = constant and for small value of α_0($0{\cdot}1 \leqslant \alpha < 0{\cdot}5$, $\alpha_0 < 4$), the latitudinal circumference decreases compared to that at the equator (i.e. equatorial circumference). Further, for the same value of α but $\alpha_0 > 4$, the latitudinal circumference increases gradually as one approaches the pole. With $\alpha = 0{\cdot}5$ and $\alpha_0 = 4$, it first increases with $y = \cos\theta$ and then decreases. The variations of A_1 are plotted in figures 7(a) and 7(b). It is observed that for small values of α_0, the equatorial circumference (A_e) is a decreasing function of α_0. However, for large values of α_0($\alpha_0 > 20$), the circumference at the equator approaches a constant as shown in figure 8.

The polar circumference is given by

$$A_p = \frac{k}{(1-\alpha^2)} \int_0^{2\pi} [\alpha^2\{(1+\cos\theta)e^{(\alpha_0/2)(2-\cos\theta)} - (1-\cos\theta)e^{(-\alpha_0/2)(2+\cos\theta)}\}^2 + 4e^{\alpha_0\cos\theta}]^{1/2} d\theta. \tag{70}$$

The evaluation of the integral (70) is difficult. However, it is found that for a constant value of α (but $\alpha < 1$) the polar circumference is an increasing function of α_0 (see figure 9). It is also noted that the rate of increase of A_p is large for greater value of α. For constant α_0, A_p increases too with α.

(c) *Gaussian curvature*

The Gaussian curvature of the metric (63) is now calculated using (41) and is expressed as

$$C = -\frac{(1-\alpha^2)^2}{2k^2}\left[\frac{B'_4}{B'_1} - \frac{1}{B'^2_1}(2B'_3B'_5 + B'_2B'_6) + \frac{2}{B'^3_1}B'_2B'^2_5\right], \tag{71}$$

where

$$B'_1 = \alpha^2(b'_1 + 2b'_2\cos\theta + b'_3\cos^2\theta) + 4e^{2\alpha_0\cos\theta},$$

$$B'_2 = \sin^2\theta e^{\alpha_0\cos\theta},$$

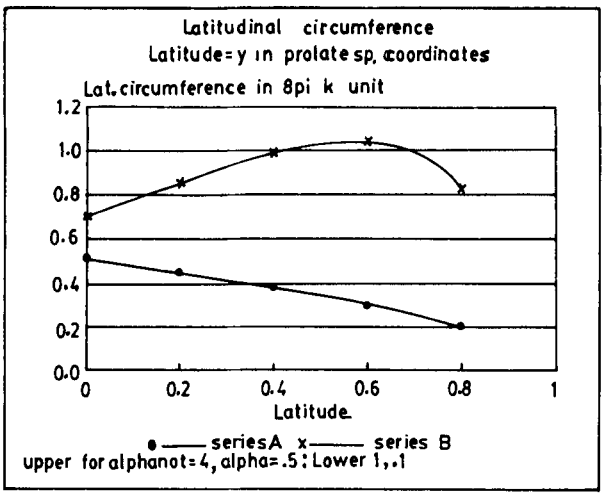

Figure 7(a). The nature of latitudinal circumferences are shown in the figure for different constant sets of values of α_0 and α. (Series B for $\alpha_0 = 4$, $\alpha = 0{\cdot}5$, and series A for $\alpha_0 = 1$, $\alpha = 0{\cdot}1$).

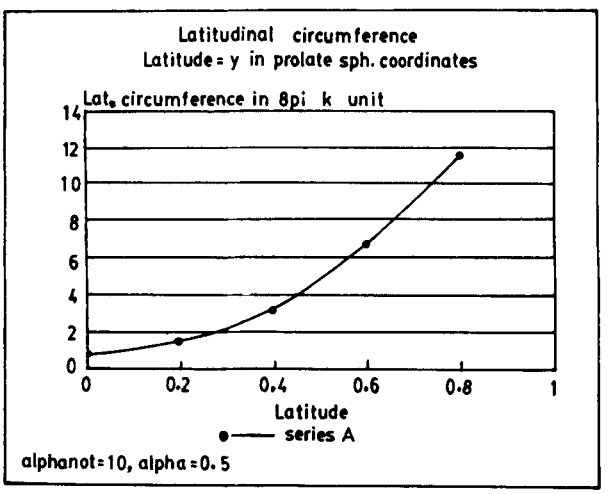

Figure 7(b). Another plot of latitudinal circumference for $\alpha_0 = 10$, $\alpha = 0{\cdot}5$. The nature of A_1 differs considerably from that shown in figure 7(a). This is due to the change in the value of α_0.

$$B'_3 = (\alpha_0 \sin^2\theta - 2\cos\theta)e^{\alpha_0 \cos\theta},$$

$$B'_4 = [\alpha_0^2 \sin^2\theta - 2(1 + 2\alpha_0 \cos\theta)]e^{\alpha_0 \cos\theta},$$

$$\dot{B'_5} = 2\alpha^2(b'_2 + b'_3 \cos\theta) + 8\alpha_0 e^{2\alpha_0 \cos\theta},$$

$$B'_6 = 2\alpha^2 b'_3 + 16\alpha_0^2 e^{2\alpha_0 \cos\theta}, \qquad (72)$$

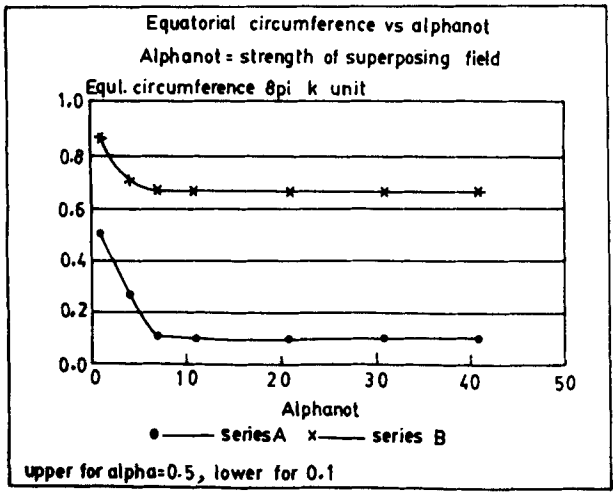

Figure 8. The graph represents the variation of equatorial circumference with the strength of the superposing field. With the increase in α_0, A_e first decreases and then assumes a constant value. The upper curve is for $\alpha = 0{\cdot}5$ and the lower one is for $\alpha = 0{\cdot}1$.

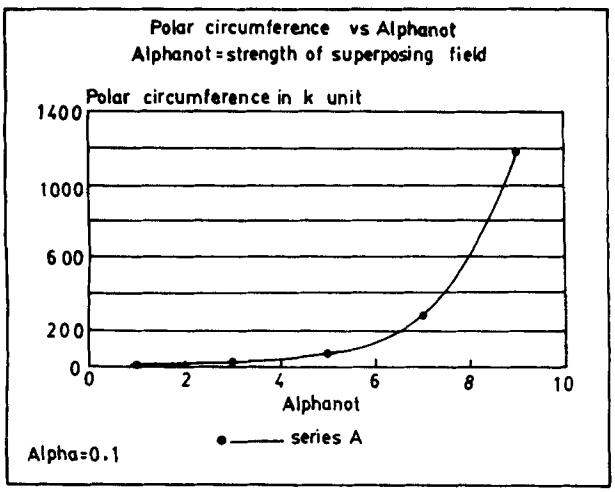

Figure 9. Variation of polar circumference (A_p) with α_0 is shown. A_p increases with the increase in α_0. The assumed value of $\alpha = 0{\cdot}1$.

and

$$b'_1 = (e^{\alpha_0} - e^{-\alpha_0})^2,$$
$$b'_2 = e^{2\alpha_0} - e^{-2\alpha_0},$$
$$b'_3 = (e^{\alpha_0} + e^{-\alpha_0})^2. \tag{73}$$

The curvature at the pole $\theta = 0$

$$C_{\theta=0} = \frac{(1-\alpha^2)^3 e^{-3\alpha_0}}{4k^2(1+\alpha^2)^2}\left[(1-2\alpha_0)e^{2\alpha_0} - \frac{2\alpha^2}{(1-\alpha^2)}\right]. \tag{74}$$

As the value of α_0 is increased, the curvature at the pole decreases. A zone of negative curvature develops around the pole $\theta = 0$, if the values of α_0 and α satisfy the following relation

$$(1-2\alpha_0)e^{2\alpha_0} < \frac{2\alpha^2}{(1-\alpha^2)} \tag{75}$$

provided $\alpha < 1$. However, when $\alpha > 1$, the condition for obtaining a negative curvature is somewhat different and it is expressed by

$$(2\alpha_0 - 1)e^{2\alpha_0} < \frac{2\alpha^2}{(\alpha^2-1)}. \tag{76}$$

The curvature at the other pole is obtained by putting $\theta = \pi$ in (71)–(72) and can be written in the form

$$C_{\theta=\pi} = \frac{(1-\alpha^2)^3 e^{3\alpha_0}}{4k^2(1+\alpha^2)^2}\left[(1+2\alpha_0)e^{-2\alpha_0} - \frac{2\alpha^2}{(1-\alpha^2)}\right]. \tag{77}$$

The curvature thus increases with increasing values of α_0. If the values of α_0 and α are such that they satisfy the following relation

$$(1+2\alpha_0)e^{-2\alpha_0} < \frac{2\alpha^2}{(1-\alpha^2)}, \tag{78}$$

a zone of negative curvature develops around the polar region $\theta = \pi$.

From the above discussion it follows that zones of negative curvature develops around the pole whether $\alpha < 1$ or $\alpha > 1$. But the restriction on the values of α_0 is different in each case. With $\alpha < 1$, the negative curvature will appear when $\alpha_0 < 1/2$ and condition (75) is obeyed. If the value of α_0 becomes $\alpha_0 \geqslant 1/2$, the curvature will then become negative irrespective of condition (75). On the other hand, when $\alpha > 1$, zone of negative curvature will appear if $\alpha_0 > 1/2$ and restriction (76) is satisfied. However, when $\alpha_0 \leqslant 1/2$, the curvature will be negative whether α_0 and α satisfy (76) or not. At the pole $\theta = \pi$, for $\alpha < 1$, as long as the inequality (78) is satisfied, there is no other restriction on the value of α_0 in obtaining negative curvature at that pole. If $\alpha > 1$, the curvature at the pole $\theta = \pi$ will always be negative.

At the equator, $\theta = \pi/2$, the curvature becomes

$$C_{\theta=\pi/2} = \frac{(1-\alpha^2)^2}{2k^2L^3}[L^2(2-\alpha_0^2) + 2L(N + 2\alpha_0 M) - 8M^2], \tag{79}$$

where

$$\begin{aligned} L &= b_1'\alpha^2 + 4, \\ M &= b_2'\alpha^2 + 4\alpha_0, \\ N &= b_3'\alpha^2 + 8\alpha_0^2. \end{aligned} \tag{80}$$

b_1', b_2', b_3' are given by (73).

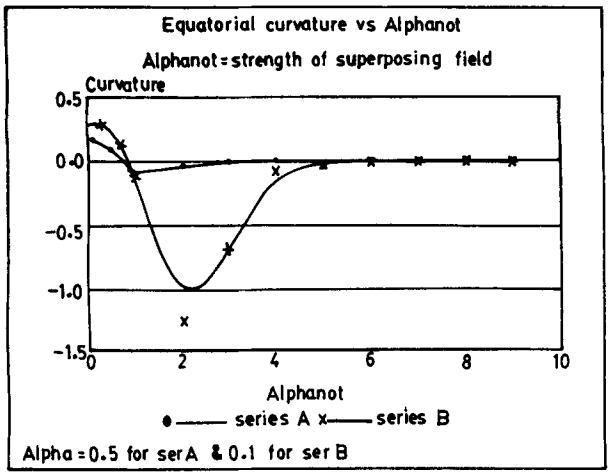

Figure 10. Plot showing the nature of variation of equatorial curvature (C_e) with α_0 for pre-assigned value of α. Here, $\alpha = 0{\cdot}5$ for series A and $\alpha = 0{\cdot}1$ for series B. C_e decreases with increase in α_0. The negative curvature region is also shown.

A computer analysis shows that the equatorial curvature decreases with the increase in α_0, and for $\alpha_0 \geq 0{\cdot}9$, a zone of negative curvature develops around the equatorial region. The variation of equatorial curvature with the strength of the superposing field α_0 and the negative curvature region are illustrated in figure 10. Further, it is observed that with the increase in α, $C_{\theta=\pi/2}$ decreases.

4. Conclusion

An analysis of the surface geometry of our derived metrics [1] is presented in this paper. In set 1, the derived metric is asymptotically flat and on imposing some restrictions on the constants α_0 and α appearing in the solutions ((21)–(26)) it reduces to the well-known Schwarzschild and Kerr metrics. The derived solution, thus generalizes the Kerr metric with an arbitrary set of multipole moments determined by the parameter α_0. The singularities of the solution are investigated using computer. The seed function is singular on the surface $x + y = 0$ and this singularity is reflected in the derived metric too. Since $1 > y > -1$, the singular values of x remain encased within $x = 1$ surface. Further the metric is singular at the poles $x = \pm 1, y = \pm 1$. It is observed that the location of singular points depend on the values of the constants α_0 and α. For large y and for $\alpha < 0{\cdot}5$, the x-coordinates of the singular points are found to be located away from the origin when the strength of the superposing field α_0 gradually increases, while for $\alpha \sim 0{\cdot}9$ and for the same value of y, the values of x are decreasing function of α_0. When the values of α_0 and y are kept constant the singular points are found to be located away from $x = 1$ value with the increment in α.

It has been stated earlier that with $\alpha_0 = 0$, our derived metric reduces to the Kerr metric. When $\alpha_0 \neq 0$, it is found that the infinite red shift surface becomes distorted although the event-horizon remains the same as that of Kerr.

The surface area is found to be an increasing function of α_0. It is also noted that both the equatorial and polar circumferences decrease with α_0 for $\alpha < 0{\cdot}6$ and both of them are found to increase with α_0 when $\alpha \geqslant 0{\cdot}6$. In the last case the rate of increase of A_e is greater than that of A_p.

In this connection, it may be pointed out that the results obtained here is contrary to our previous result [16], where the same seed has been used to obtain two soliton solution of axially symmetric metric by the inverse scattering method of Belinskii and Zakharov [17]. It was found that A_p increases with α_0 while A_e decreases. This is perhaps due to a greater number of constants appearing in the solution [16] and different sets of values assigned to the constants. However, when the constants are properly adjusted, it is found that the solutions obtained by these two methods (viz. the Gutsunaev and Manko method of the present paper and the inverse scattering method of [16]) coincide with each other.

The Gaussian curvatures of metric (30) are also evaluated. On imposing some restrictions on the constants α_0 and α, zones of negative curvature are found to develop around the polar region.

The coordinate invariant Geroch–Hansen relativistic mass and angular momentum multipole moments are computed and their relative abundances are plotted. On substituting $\alpha_0 = 0$, the multipole moments reduce to the moments corresponding to Kerr.

For set 2, it was shown that with proper restrictions on the constants α_0 and α, our solutions given in (56)–(61) reduce to the Schwarzschild, Kerr and Kerns and Wild metrics. The general solution may thus be interpreted as the non-linear super-position of Kerr metric with a gravitational field. The solutions obtained in this case are not asymptotically flat. The event-horizon is always covered by the infinite red shift surface. The metric is singular at the poles $x = \pm 1$, $y = \pm 1$ and at least one singular point exists on the equatorial plane.

The surface area of the event-horizon, the latitudinal and polar circumferences are evaluated and these are found to vary with α_0. The Gaussian curvatures in the polar and equatorial regions are also computed and it is noted that when certain restrictions are imposed on the constants α_0 and α, zones of negative curvature develop around those regions.

In the late sixties, Kerr–Newman solution drew much attention of the astrophysicists, since that was the only solution then, supposed to represent the actual field of a rotating charged object. Moreover, that solution goes over to Kerr when electrostatic charge is set to zero.

It is now believed that Kerr metric cannot represent the exact exterior field of an arbitrary rotating star because of its very special relationship between the multipole moments and angular momentum [18]. In our previous paper we have given a Kerr-like metric associated with/without external gravitational field. In this paper, we studied their structural properties in order to compare them with Kerr metric. Although our analysis is a positive step towards the goal, it is not proved beyond doubt whether these solutions prove or disprove Israel and Caster conjecture [19, 20, 21] and describe the exterior field of a so called black hole. As regards naked singularities, Newton–Rapson or equivalent methods of analysis failed to predict naked singularity outside the infinite red shift surface. Further analysis remains open for future.

Acknowledgements

Thanks are due to Prof. S Banerji, Department of Physics, Burdwan University, Burdwan for many useful discussions on the paper. One of the authors (SC) wishes to thank the UGC for financial support.

References

[1] K C Das and S Chaudhuri, *Pramana – J. Phys.* **40**, 277 (1993)
[2] R P Kerr, *Phys. Rev. Lett.* **11**, 237 (1963)
[3] R M Kerns and W J Wild, *Gen. Relativ. Gravit.* **14**, 1 (1982)
[4] R Geroch, *J. Math. Phys.* **11**, 1955 (1970)
[5] R Geroch, *J. Math. Phys.* **11**, 2580 (1970)
[6] R O Hansen, *J. Math. Phys.* **15**, 46 (1974)
[7] H Quevedo, *Phys. Rev.* **D39**, 2904 (1989)
[8] C Hoenselaers, Gravitational collapse and relativity, *Proc. 14th Yamada Conf.*, Kyoto Japan, 1986, edited by H Sato and T Nakamura (World Scientific, Singapore, 1986) p. 176–184
[9] F J Ernst, *Phys. Rev.* **D167**, 1175 (1968)
[10] E J Ernst, *Phys. Rev.* **D168**, 1415 (1968)
[11] Ts I Gutsunaev and V S Manko, *Gen. Relativ. Gravit.* **20**, 327 (1988)
[12] W Kinnerseley and M Walker, *Phys. Rev.* **D2**, 1359 (1970)
[13] W J Wild and R M Kerns, *Phys. Rev.* **D21**, 332 (1980)
[14] T Willmore, *An introduction to differential geometry* (Oxford University Press, Oxford, England, 1959) p. 79
[15] V S Manko and I D Novikov, *Class. Quant. Gravit.* **9**, 2477 (1992)
[16] S Chaudhuri and K C Das, (Communicated)
[17] V A Belinskii and V E Zakharov, *Sov. Phys. JETP*, **48**, 985 (1978)
[18] J Castejon–Amenedo and V S Manko, *Phys. Rev.* **D41**, 2018 (1990)
[19] W Israel, *Phys. Rev.* **164**, 1776 (1967)
[20] B Carter, *Phys. Rev. Lett.* **26**, 331 (1971)
[21] K S Throne, *Comm. Astrophys. Space Phys.* **2**, 191 (1970)